Journal of Organometallic Chemistry 695 (2010) 1293–1299

Contents lists available at ScienceDirect

Journal of Organometallic Chemistry

journal homepage: www.elsevier.com/locate/jorganchem

Electronic structures of organometallic complexes of f elements LXXIII: Parametric analysis of the crystal field splitting pattern of tris(η^5-pentamethylcyclopentadienyl)cerium(III) ☆

Hanns-Dieter Amberger [a,*], Hauke Reddmann [a], Thomas J. Mueller [b], William J. Evans [b]

[a] Institut für Anorganische und Angewandte Chemie der Universität Hamburg, Martin-Luther-King-Platz 6, 20146 Hamburg, Germany
[b] Department of Chemistry, University of California, Irvine, California 92697-2025, USA

ARTICLE INFO

Article history:
Received 15 December 2009
Accepted 17 February 2010
Available online 23 February 2010

Keywords:
Cerium
Substituted cyclopentadienyl ligand
Low temperature MIR spectrum
Paramagnetic susceptibility
Crystal field analysis

ABSTRACT

By comparing the far infrared (polyethylene pellets, room temperature) and mid-infrared spectra (KBr pellets, room temperature and ca. 90 K) of pseudo trigonal planar Ce(η^5-C_5Me_5)$_3$ (**1**) with the corresponding ones of La(η^5-C_5Me_5)$_3$ (**2**) and considering the low temperature paramagnetic susceptibility data of **1** the crystal field (CF) splitting pattern of **1** could be derived. The free parameters of a phenomenological Hamiltonian were fitted to this pattern achieving an r.m.s. deviation of 8.9 cm^{-1} for seven assignments. The fact that the difference of the experimental energies of the barycenters of CF levels of the multiplets $^2F_{7/2}$ and $^2F_{5/2}$ is larger than in the gaseous free Ce^{3+} ion (experimental "anti"-relativistic nephelauxetic effect) could be explained by coupling effects of these multiplets via the CF, resulting in a lower spin–orbit coupling parameter than in the case of the free gaseous Ce^{3+} ion. The experimental CF splitting pattern of **1** is compared to the results of a relativistic DV-Xα calculation on the pseudo trigonal planar model compound Ce(η^5-C_5H_5)$_3$. In addition, the prediction of the energies of f → d and charge transfer transitions of Ce(η^5-C_5H_5)$_3$ are compared to the absorption and luminescence spectra of complex **1**.

1. Introduction

In spite of their simple 4f^1 configuration, the electronic structures of Ce^{III} compounds rarely have been the target of crystal field (CF) analyses [2–5]. The main reason for this is that the combined spin–orbit and CF effects produce CF levels which have to be detected in the far infrared (FIR) and mid-infrared (MIR) ranges. These ranges, however, are dominated by signals of vibrations which are – at least at room temperature – much stronger than those of the f → f transitions that are sought [2–5]. At low temperatures, these signals usually get noticeably stronger and are frequently shifted in energy by 5–15 cm^{-1}, thus delivering an additional criterion for their identification beside the common way of comparing the FIR and MIR spectra of the Ce^{III} compound of interest with those of the corresponding "optically empty" La^{III} compound [2–5].

In very rare cases, Ce^{III} compounds exhibit electronic Raman transitions [6–8], but usually only at lower temperatures. If suitable single crystals are available, the polarization properties of these transitions possibly allow their assignments to be made.

During the latest decades, both methods were also applied to some organometallic Ce^{III} complexes, but with very different success. [(η^8 – C_8H_8)Ce(Tp^{Me_2})(THF)] (Tp^{Me_2} = hydrotris(3,5–dimethylpyrazolyl)borate) exhibited no f–f transitions, neither in the FIR/MIR nor in the Raman spectrum, even at low temperatures [9]. Transitions were observed, however, for [(η^5-C_5H_5)$_3$Ce(THF)], in the MIR spectrum (450, 2135, 2220, 2465 cm^{-1}) at low temperatures [10]. [(η^5-C_5H_5)$_3$Ce(NCCH$_3$)$_2$] showed signals of f–f origin in both the MIR (2128, 2152 cm^{-1}) and Raman spectrum (320, 2129, 2154 cm^{-1}) at ca. 30 K [11]. Ce(η^5-C_5Me_4H)$_3$ displayed a spectrum only in the MIR range (890, 2135, 2360, 2480, 3875 cm^{-1}) even at ambient temperature [12].

The last finding as well as the detection of electronic Raman transitions in the case of $SmCp^*_3$ [13] (Cp^* = η^5-C_5Me_5) and $PrCp^*_3$ [1] encouraged us to derive the experimental CF splitting pattern of pseudo (ψ) trigonal planar $CeCp^*_3$ (**1**) (see Fig. 1) by comparing the FIR/MIR (pellets) and Raman spectra (oriented single crystals) of **1** with those of $LaCp^*_3$ (**2**).

If sufficient CF levels are detected, the free parameters of a phenomenological Hamiltonian can be fitted to the experimentally derived CF splitting pattern. The parameters obtained allow the insertion of $CeCp^*_3$ into empirical spectrochemical and relativistic nephelauxetic series [14] and the set-up of the experimentally oriented non-relativistic molecular orbital (MO) scheme of **1** (in the f range [15]), which can be compared with the results of a previous

☆ For part LXXII, see Ref. [1].

* Corresponding author. Tel.: +49 40 42838 3524; fax: +49 40 42838 2893.
E-mail address: fc3a501@uni-hamburg.de (H.-D. Amberger).

0022-328X/$ - see front matter © 2010 Elsevier B.V. All rights reserved.
doi:10.1016/j.jorganchem.2010.02.018

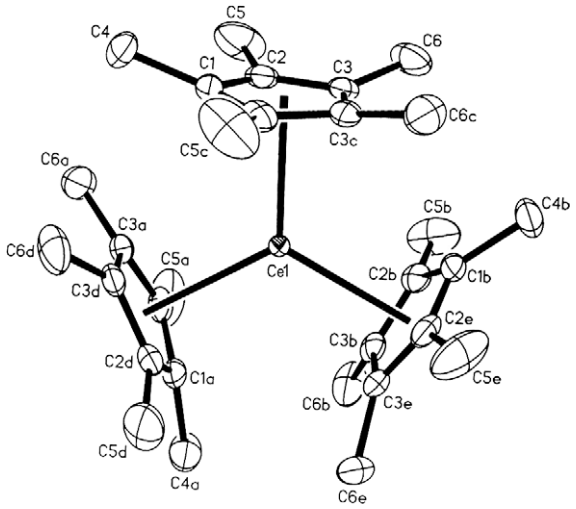

Fig. 1. Molecular structure of $CeCp^*_3$ in the crystal (adapted from $PrCp^*_3$ [1]).

non-relativistic SW-Xα calculation on the ψ trigonal planar model complex $Ce(\eta^5\text{-}C_5H_5)_3$ [16]. Likewise, the predicted CF splitting pattern of $Ce(\eta^5\text{-}C_5H_5)_3$ [17] (relativistic DV-Xα approximation) as well as the predictions of the energies of f → d and charge transfer transitions [17] can be compared with the experimental findings of **1**.

2. Experimental

Small single crystals of dark green **1** [18] and yellow **2** [19] were synthesized at University of California, Irvine, according to the literature. The absorption spectra in the FIR (polyethylene pellets), MIR (KBr pellets) and NIR/vis (unoriented single crystals, KBr pellets) ranges were recorded by means of the instruments Vertex 70 (Bruker), FT-IR 1720 (Perkin–Elmer) and Cary 5e (Varian), respectively. The latter two can be combined with a transfer cryostat Helitran LT-3-110 (Air Products) and the Cary 5e apparatus additionally with a bath cryostat, using liquid N_2 or liquid He as coolant. For running the Raman spectra (powdered material and single crystals sealed in glass tubes), the recently developed Senterra instrument (Bruker) equipped with a microscope and lasers with excitation lines at 785, 632.8 and 532 nm was available. Paramagnetic susceptibility was determined on a Quantum Design vibration sample SQUID magnetometer.

3. Phenomenological Hamiltonian, symmetry considerations and selection rules

The energy levels within f^1 configuration in D_{3h} symmetry can be written in terms of the atomic free ion (H_{FI}) and crystal field (H_{CF}) Hamiltonian as follows:

$H = H_{FI} + H_{CF}$, where
$H_{FI} = a_{SO}\zeta_{4f}$ [4, p. 67], and
$H_{CF}(D_{3h}) = B_0^2C_0^{(2)} + B_0^4C_0^{(4)} + B_0^6C_0^{(6)} + B_6^6(C_{-6}^{(6)} + C_6^{(6)})$ [4, p. 242].

ζ_{4f} presents the radial part of the spin–orbit interactions, while a_{SO} is its angular part. The CF interaction for the above symmetry is represented by the B_q^k parameters and the tensor operators $C_q^{(k)}$ [4, p. 170].

A CF of D_{3h} symmetry splits the ground multiplet $^2F_{5/2}$ of Ce^{III} compounds into the CF levels $1\Gamma_7$, $1\Gamma_8$, and $1\Gamma_9$, respectively, and the excited multiplet $^2F_{7/2}$ (3.5 ζ_{4f} higher) into $2\Gamma_7$, $3\Gamma_7$, $2\Gamma_8$ and $2\Gamma_9$ [4, p. 265]. In case of powdered or dissolved material the selection rules of Table 1 hold for induced electric dipole transitions between these levels.

4. Results and discussion

4.1. Derivation and simulation of the CF splitting pattern

In Fig. 2, the FIR spectra of compounds **1** and **2** are presented. Obviously, the spectra are very similar, but because of the more concentrated pellet of **1**, some shoulders and weak signals are more pronounced. This probably also holds for the weak signal at 94 cm^{-1}, which does not appear in the FIR spectrum of **2**, but could be observed in the case of $SmCp^*_3$ [13].

At room temperature, the MIR spectrum of **1** shows in the range 750–1000 cm^{-1} a broad asymmetric band with the minimum at ca. 882 cm^{-1} beside two sharper signals at 803 and 946 cm^{-1} (see Fig. 3). At low temperatures, the two sharper signals get somewhat stronger and are weakly shifted to 806 and 947 cm^{-1} (and additional shoulders at 801 and 943 cm^{-1} appear), whereas the above-mentioned broad band increases considerably and the minimum is shifted to 866 cm^{-1} (besides, two additional shoulders can be observed at 870 and 876 cm^{-1}) (see Fig. 3). These findings suggest that the former signals are of vibrational and the latter of electronic origin. This is additionally supported by the nonexistence of the f → f band and the nearly identical band shapes and energies of the vibrational signals in the low temperature MIR spectrum of **2** (see Fig. 3). The most plausible explanation for the shoulder at 876 cm^{-1} and the electronic band at 866 cm^{-1} would be that they correspond to transitions initiating at the CF ground state and the first excited level which are separated by approximately 10 cm^{-1}, whereas the shoulder at 870 cm^{-1} is produced by the superposition of the bell-shaped signals of the above-mentioned two electronic transitions and, like in the case of 2, a vibrational signal.

In the range 2000–2600 cm^{-1} three asymmetric signals at 2170, 2360 and 2490 cm^{-1} appear in the room temperature MIR spectrum of **1** (see Fig. 4). At low temperatures, the minima of these signals are shifted to 2148, 2346 and 2470 cm^{-1} with accompanying shoulders at 2155, 2360 and 2475 cm^{-1} (see Fig. 4). None of these signals are present in the low temperature MIR spectrum of **2** and are thus of electronic origin. Again, these findings are correlated with transitions initiating from the CF ground state and a first excited level lying some 10 cm^{-1} higher.

An additional weak and broad signal with the minimum at ca. 3675 cm^{-1} can be detected in the MIR spectrum of **1** recorded at ambient temperature. At low temperatures, this signal increases and splits into two components at 3682 and 3693 cm^{-1}, thus again confirming the existence of a first excited level approximately 10 cm^{-1} above the CF ground state. As before, none of these signals appear in the corresponding spectrum of **2** (see Fig. 5).

In case of the similarly trigonal planar $Ce(\eta^5\text{-}C_5Me_4H)_3$ [20] the energetic sequence $1\Gamma_8 \sim 1\Gamma_9 < 1\Gamma_7 \ll 2\Gamma_9 < 2\Gamma_8 < 2\Gamma_7 \ll 3\Gamma_7$ of CF levels was concluded from MIR measurements [12]. The same sequence will probably hold for the higher, energetically well separated CF levels of **1**. Hence the levels $1\Gamma_7$, $2\Gamma_9$, $2\Gamma_8$, $2\Gamma_7$ and $3\Gamma_7$

Table 1
Selection rules for transitions of induced electric dipole character of powdered or solved f^n systems (n odd) which are exposed to a CF of D_{3h} symmetry (from Ref. [4], p. 255).

D_{3h}	Γ_7	Γ_8	Γ_9
Γ_7	–[a]	+	+
Γ_8	+	–	+
Γ_9	+	+	+

[a] + allowed, – forbidden.

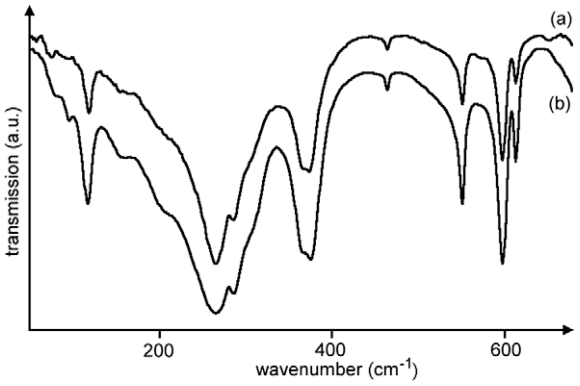

Fig. 2. FIR spectra of $LnCp^*_3$ in the range 50–650 cm^{-1} (room temperature, polyethylene pellets): (a) Ln = La; (b) Ln = Ce.

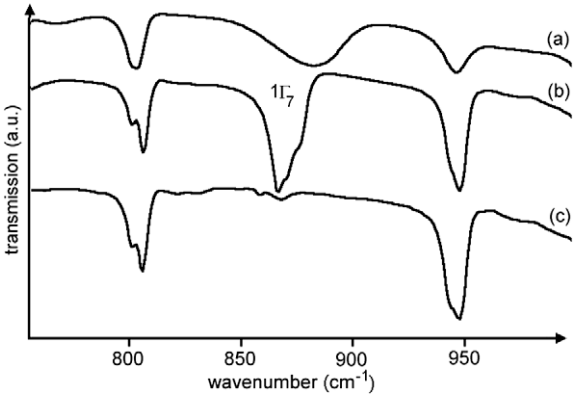

Fig. 3. MIR spectra of $LnCp^*_3$ in the range 750–1000 cm^{-1} (KBr pellets): (a) Ln = Ce, room temperature; (b) Ln = Ce, ca. 90 K; (c) Ln = La, ca. 90 K.

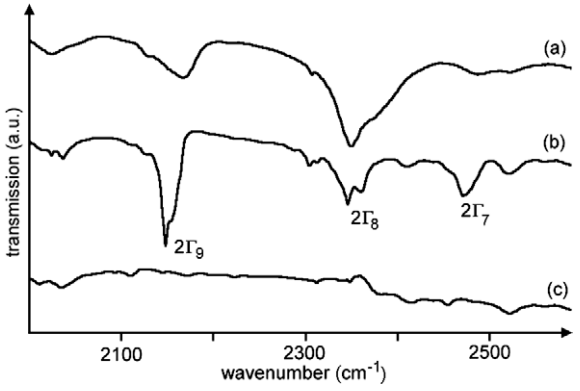

Fig. 4. MIR spectra of $LnCp^*_3$ in the range 2000–2600 cm^{-1} (KBr pellets): (a) Ln = Ce, room temperature; (b) Ln = Ce, ca. 90 K; (c) Ln = La, ca. 90 K.

of compound **1** are correlated with the CF energies of 876, 2155, 2360, 2475 and 3693 cm^{-1}, respectively (see Figs. 2–5).

The symmetries of the CF ground and first excited state, however, are uncertain at the present stage. $Ce(\eta^5\text{-}C_5Me_4H)_3$ and $Ce(\eta^5\text{-}C_5H_4t\text{-}Bu)_3$ have a CF ground state of Γ_8, and a first excited level of Γ_9 symmetry [12], whereas a non-relativistic SW-Xα [16] and a relativistic DV-Xα [17] calculation for the ψ trigonal planar model complex $Ce(\eta^5\text{-}C_5H_5)_3$ resulted in a reversed sequence (vide infra).

The combinations of $E(1\Gamma_8) = 0\ cm^{-1}$, $E(1\Gamma_9) = 10\ cm^{-1}$ and $E(1\Gamma_9) = 0\ cm^{-1}$, $E(1\Gamma_8) = 10\ cm^{-1}$ with the above-mentioned sequence of higher energies of compound **1** are denoted as CF splitting patterns A and B, respectively. According to the selection rules for induced electric dipole transitions (see Table 1), all possible transitions initiating at $1\Gamma_8$ and $1\Gamma_9$ to the remaining CF states of the f^1 configuration are allowed, with the exception of the transition $1\Gamma_8 \rightarrow 2\Gamma_8$. In contrast to the selection rules, the transition $1\Gamma_8/1\Gamma_9 \rightarrow 2\Gamma_8$ corresponds to two signals at 2346 and 2360 cm^{-1}, thus not allowing the identification of the symmetries of CF ground state and first excited level on the basis of the MIR spectrum.

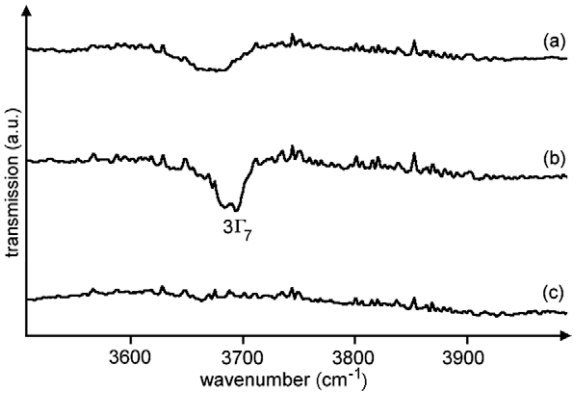

Fig. 5. MIR spectra of $LnCp^*_3$ in the range 3500–4000 cm^{-1} (KBr pellets): (a) Ln = Ce, room temperature; (b) Ln = Ce, ca. 90 K; (c) Ln = La, ca. 90 K.

In order to elucidate whether CF splitting pattern A or B is the proper one, we planned to study both the polarization properties of electronic Raman transitions [21] of oriented single crystals and the magnetic properties of powdered material of **1** at low temperatures. The polarized Raman measurements, however, showed instead of the desired electronic transitions only vibrational transitions (comparable to those of $SmCp^*_3$ [13]), partly superimposed on broad luminescence transitions (vide infra).

In order to identify the proper CF splitting pattern on the basis of paramagnetic susceptibility measurements, the free parameters of the above described phenomenological Hamiltonian were fitted to the CF splitting patterns A and B, respectively (rms values of 8.9 and 1.9 cm^{-1} for seven assignments). Subsequently, the μ^2_{eff} values at ca. 0 K were calculated on the basis of van Vleck's formula [22] (for both patterns, making use of the wavefunctions and eigenvalues of the two fits. In order to consider possible covalency effects, the conventional Zeeman operator was replaced in the calculations by $k\vec{L} + 2\vec{S}$ (k orbital reduction factor [23]). The calculations lead for CF splitting pattern A to μ^2_{eff} values between 3.54 and 3.32 μ^2_B for orbital reduction factors between 1.0 and 0.975, whereas CF splitting pattern B is connected with considerably lower values between 1.80 and 1.69 μ^2_B.

In the range 3.4–10 K, the temperature dependence of μ^2_{eff} of **1** is nearly linear and the extrapolation of this line versus $T = 0$ K meets the μ^2_{eff} axis at 3.48 μ^2_B. Hence, CF splitting pattern A (see Table 2, column 5) is the proper one. The corresponding parameter set is given in Table 3.

The parameter $N_v/\sqrt{4\pi} = \sqrt{\sum_{k,q}(B^k_q)^2/(2k+1)}$ is considered as a relative measure of the CF strength experienced by the central Ln^{3+} ion [25]. Inserting the CF parameters of **1** into this relation, one ends up with an $N_v/\sqrt{4\pi}$ value of 1333 cm^{-1}. In Table 4, this value is compared to those of other Ce^{III} compounds. Obviously, the central ion of complex **1** experiences the fourth highest CF strength found to date for Ce^{III} compounds (see Table 4). Like in the pairs of compounds $LnCp^*_3/Ln(C_5Me_4H)_3$ (Ln = Pr, Sm) the $N_v/\sqrt{4\pi}$ value of **1** is lower than that of $Ce(C_5Me_4H)_3$ (see Tables 3 and 4), which is presumably caused by the larger Ln–C distances

Table 2
Comparison of experimental and fitted CF energies of $CeCp^*_3$ as well as results of relativistic and non-relativistic quantum chemical calculations on the model complex $Ce(\eta^5\text{-}C_5H_5)_3$. All values in cm^{-1}.

Multiplet	CF level		*E* (fit.)	*E* (exp.)	*E* (calc.)[a]	*E* (calc.)[b]
$^2F_{5/2}$[c]	$1\Gamma_8$[d]	±1/2[e]	0	0	97	245
$^2F_{5/2}$	$1\Gamma_9$	±3/2	7	10	0	0
$^2F_{5/2}$	$1\Gamma_7$	±5/2	870	876	274	832
$^2F_{7/2}$	$2\Gamma_9$	±3/2	2150	2155	2574	2314
$^2F_{7/2}$	$2\Gamma_8$	±1/2	2356	2360	3901	2553
$^2F_{7/2}$	$2\Gamma_7$	±5/2	2483	2475	2915	2264
$^2F_{7/2}$	$3\Gamma_7$	±7/2	3694	3693	7355	5851

[a] Result of a relativistic DV-Xα calculation [17].
[b] Result of a non-relativistic SW-Xα calculation [16] combined with ζ_{4f} = 640 cm^{-1} [12].
[c] Dominating Russell–Saunders multiplet $^{2S+1}L_J$.
[d] The Bethe Γ notation for the double group D'_{3h} is used. The irreps Γ_i are ordered in ascending energy.
[e] Largest eigenvector component $\pm M_J$.

Table 3
Comparison of the parameter values of $LnCp^*_3$ (Ln = Ce, Pr, Sm) as well as of relativistic and non-relativistic quantum chemical calculations on the model complex $Ce(\eta^5\text{-}C_5H_5)_3$. All values in cm^{-1}.

Parameter	$CeCp^*_3$	$Ce(\eta^5\text{-}C_5H_5)_3$[a]	$Ce(\eta^5\text{-}C_5H_5)_3$[b]	$PrCp^*_3$[c]	$SmCp^*_3$[d]
F^2	–	–	–	66 569	71 817
F^4	–	–	–	49 886	56 751
F^6	–	–	–	33 439	36 292
ζ_{4f}	641	806	–	746	1129
α	–	–	–	[23.1][e]	[21.6]
β	–	–	–	[−757]	[−724]
γ	–	–	–	[1534]	[1700]
T^2	–	–	–	–	[291]
T^3	–	–	–	–	[13]
T^4	–	–	–	–	[34]
T^6	–	–	–	–	[−193]
T^7	–	–	–	–	[288]
T^8	–	–	–	–	[330]
M^0	–	–	–	[1.76]	[2.4]
M^2	–	–	–	[0.99]	[1.34]
M^4	–	–	–	[0.67]	[0.91]
P^2	–	–	–	[275]	[341]
P^4	–	–	–	[206]	[256]
P^6	–	–	–	[138]	[171]
B^2_0	−2189	−3472	−3587	−2293	−2741
B^4_0	1615	4082	3647	811	1341
B^6_0	896	4443	23	1051	1556
B^6_6	−1741	−8868	−5806	−2146	−2626
$N_v/\sqrt{4\pi}$	1333	4228	3039	1385	1717
σ	8.9 (7)[f]	11.9 (7)	0 (4)	10.2 (18)	15.0 (21)

[a] Result of a relativistic DV-Xα calculation [17].
[b] Result of a non-relativistic SW-Xα calculation [16].
[c] From Ref. [1].
[d] From Ref. [13].
[e] Values in brackets held fixed on the values of $LaCl_3:Pr^{3+}$ resp. $LaCl_3:Sm^{3+}$ [24].
[f] Number of fitted energies in parentheses.

Table 4
ζ_{4f}, ζ_{4f}' and $N_v/\sqrt{4\pi}$ values of various Ce^{III} compounds. All values in cm^{-1}.

Compound	ζ_{4f}	ζ_{4f}'	$N_v/\sqrt{4\pi}$	Ref.
Ce^{3+}	643.7	643.7	–	[30]
$LaCl_3:Ce^{3+}$	627	633	341	[31]
$LaCl_3:Ce^{3+}$	627	633	356	[32]
$LaF_3:Ce^{3+}$	647	665	690[a]	[33]
$Cs_2NaCeCl_6$	635	644	867	[8]
$Cs_2NaCeCl_6$[b]	623	644	948	[34]
$Ce(C_5Me_5)_3$	641	679	1333	This work
$Ce(C_5Me_4H)_3$	640	692	1508	[12]
$Ce(\eta^5\text{-}C_5H_5)_3$[c]	640	825	3039	[12]
$Ce(\eta^5\text{-}C_5H_5)_3$[d]	806	1161	4230	[17]
$Y_3Ga_5O_{12}:Ce^{3+}$	616	690	1548	[35]
$Y_2O_3:Ce^{3+}$	620	–	1692	[36]

[a] The CF parameters given in Ref. [33] were adopted from $LaF_3:Pr^{3+}$ [33].
[b] Fitted to the experimental CF energies of Ref. [8].
[c] Result of a non-relativistic SW-Xα calculation [16] combined with ζ_{4f} = 640 cm^{-1}, from Ref. [12].
[d] Result of a relativistic DV-Xα calculation [17].

of $LnCp^*_3$ compounds [18,26,27] compared to those of $Ln(C_5Me_4H)_3$ complexes [19,28,29]. The same reason presumably holds for the decreasing CF strength going from $SmCp^*_3$ via $PrCp^*_3$ to $CeCp^*_3$ (see Table 3).

The ζ_{4f} value of **1** is somewhat larger than that of $Ce(C_5Me_4H)_3$ but lower than that of the gaseous free Ce^{3+} ion (see Table 4).

In the frame of a first-order CF calculation (neglect of the coupling of the multiplets $^2F_{5/2}$ and $^2F_{7/2}$ via the CF) the spin–orbit coupling parameter ζ'_{4f} is estimated by dividing the difference of the experimental barycenters of both multiplets by 3.5. Because of relativistic nephelauxetic effects it was originally assumed that the thus calculated ζ'_{4f} values of Ce^{III} compounds are lower than that of the gaseous Ce^{3+} ion (643.7 cm^{-1} [30]) [2]. For this reason, Dieke found fault with the ζ'_{4f} values of $LaCl_3:Ce^{3+}$ (669 cm^{-1}; the result of a miscalculation, the correct value is 633 cm^{-1} [12]) and $Yb_3Ga_5O_{12}:Ce^{3+}$ (690 cm^{-1} [35]) and declared these values as consequence of a misinterpretation of IR spectra [2, p. 139]. Compound **1** and $Ce(C_5Me_4H)_3$ have ζ'_{4f} values of 679 and 692 cm^{-1}, respectively (see Table 4). These on initial examination experimental "anti"-relativistic nephelauxetic effects could be explained in [12] by the coupling of the multiplets $^2F_{5/2}$ and $^2F_{7/2}$ via the CF, leading to lower values of ζ_{4f} than 643.7 cm^{-1}, if the phenomenological Hamiltonian for the whole f^1 configuration is used (see Table 4). In case of compounds of D_{3h} symmetry the enlargement of ζ'_{4f} (compared to ζ_{4f}) is mainly caused by the CF parameters $|B^6_6|$ and $|B^6_0|$, and to a lesser content also by $|B^2_0|$ and $|B^4_0|$ (see [12, Fig. 4]). First of all, the CF parameter $|B^6_6|$ but also $|B^6_0|$ of **1** are considerably lower than that of $Ce(C_5Me_4H)_3$ [12, Table 3]. Hence the difference $\zeta'_{4f} - \zeta_{4f}$ of **1** is with 38 cm^{-1} noticeably lower than that of $Ce(C_5Me_4H)_3$ (52 cm^{-1}, see Table 4).

4.2. Comparison of experimental and predicted electronic structures

Kaltsoyannis and Bursten calculated the relativistic MO scheme of the ψ trigonal planar model complex $Ce(\eta^5\text{-}C_5H_5)_3$ on the basis of the DV-Xα approximation [17], where the energies of the relativistic f type MOs correspond to the calculated CF splitting pattern of this compound. According to this calculation, the CF ground state is of Γ_9 symmetry, and the remaining CF levels of Γ_8 and Γ_7 symmetry of the ground multiplet $^2F_{5/2}$ have energies of 97 and 274 cm^{-1} [17]. The energies of the CF states of the excited multiplet $^2F_{7/2}$ are not explicitly mentioned, but the transitions initiating from the thermally populated levels $1\Gamma_9$, $1\Gamma_8$ and $1\Gamma_7$ of $^2F_{5/2}$ and terminating at $2\Gamma_9$, $2\Gamma_7$, $2\Gamma_8$ and $3\Gamma_7$ have energies of 2450, 2791, 3777 and 7231 cm^{-1}, respectively (see Ref. [17], Table 2). Hence, we add these wavenumbers to the barycenter of the CF energies of $^2F_{5/2}$ (124 cm^{-1}), and end at the calculated CF splitting pattern of $Ce(\eta^5\text{-}C_5H_5)_3$ as given in Table 2, column 6. In Fig. 6, the predicted CF splitting pattern of $Ce(\eta^5\text{-}C_5H_5)_3$ is compared to the experimental ones of complex **1** and $Ce(C_5Me_4H)_3$ [12]. Obviously, the calculated CF splitting pattern is by a factor of ca. two larger than the experimental ones, the predicted CF ground state is dominated by $M_J = |\pm 3/2\rangle$ instead of $|\pm 1/2\rangle$ and the levels $2\Gamma_8$ and $2\Gamma_7$ are interchanged. Fitting the free parameters of the phenomenological Hamiltonian (vide supra) to the calculated CF splitting pattern of $Ce(\eta^5\text{-}C_5H_5)_3$ one arrives at the parameter set as given in Table 3, column 3. Obviously, both the absolute values of the CF parameters (and hence also the $N_v/\sqrt{4\pi}$ value of 4228 cm^{-1}) and

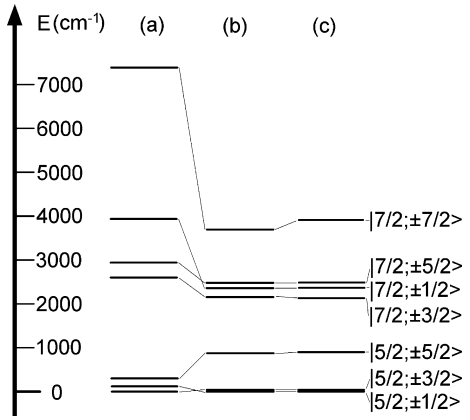

Fig. 6. Crystal field splitting patterns of $CeCp'_3$: (a) Cp′ = C_5H_5 (model complex), result of a relativistic DV-Xα calculation [17]; (b) Cp′ = Cp*, experimental; (c) Cp′ = C_5Me_4H, experimental.

ζ_{4f} (806 cm^{-1}) are much too large. This is also reflected by the unusual high difference $\zeta'_{4f} - \zeta_{4f}$ = 355 cm^{-1}.

The eigenvalues of an energy matrix of the spin-free f^1 system, into which the CF parameters of a previous parametric analysis of the compound of interest had been inserted, were defined as the experimentally-based non-relativistic MO scheme of this compound in the f range [17].

In Fig. 7, the experimentally-based non-relativistic MO schemes (in the f range) of complexes **1** and **2** are compared with the non-relativistic MO scheme of the ψ trigonal planar model complex $Ce(\eta^5\text{-}C_5H_5)_3$ calculated in the framework of the non-relativistic SW-Xα approximation [16]. Obviously, the calculated total splitting of f orbitals is considerably larger than the experimentally-based one.

The CF parameters resulting from a fit of the MO scheme of $Ce(\eta^5\text{-}C_5H_5)_3$ (in the f range [12]), based on the non-relativistic SW-Xα [16] are given in Table 3, column 4. In [12], the "non-relativistic" CF splitting pattern of $Ce(\eta^5\text{-}C_5H_5)_3$ was calculated making use of this set of CF parameters and the ζ_{4f} value of 640 cm^{-1} (see Table 2, column 7). Obviously, the non-relativistic SW-Xα approximation produces the total splitting of the ground multiplet $^2F_{5/2}$ much better than the relativistic DV-Xα calculation, but the sequence of CF levels of the excited multiplet $^2F_{7/2}$ differs even more from the experimental one.

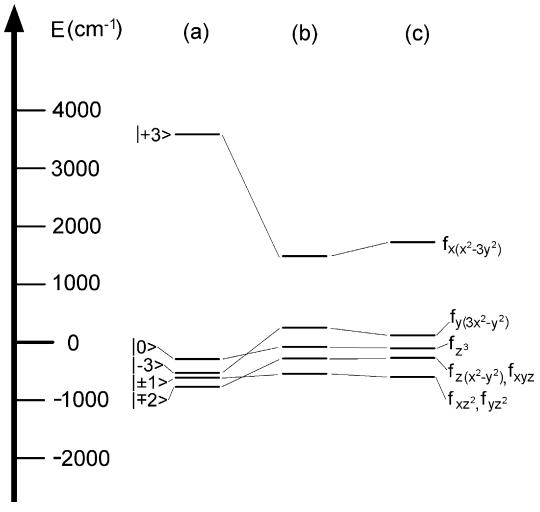

Fig. 7. Experimentally-based and calculated non-relativistic MO schemes of $CeCp'_3$: (a) Cp′ = C_5H_5 (model complex), result of a non-relativistic SW-Xα calculation [16]; (b) Cp′ = Cp*, experimental; (c) Cp′ = C_5Me_4H, experimental.

According to Kaltsoyannis and Bursten, it is not expected that substitution of the H atoms of the η^5-C_5H_5 rings with other groups should have a pronounced effect upon the essentially metal-localized electronic promotions [17]. For this reason, the strong difference between experimental and calculated CF splitting patterns cannot simply be explained by the fact that the experimental work was done with $CeCp^*_3$ and the calculations on $Ce(\eta^5\text{-}C_5H_5)_3$.

In the frame of the above-mentioned relativistic DV-Xα calculation, not only the energies of f → f but also of the lowest (zero phonon) $^2F_{5/2} \rightarrow 5d$ (16 542 cm^{-1}) as well as of the charge transfer transitions $(\eta\text{-}C_5H_5)\pi_2 \rightarrow {}^2F_{5/2}$ (26 554 cm^{-1}) and $^2F_{5/2} \rightarrow (\eta\text{-}C_5H_5)\pi_3$ with admixtures of 5d (27 660 cm^{-1}) were predicted [17, Table 2].

In order to check the above predicted relativistic transition energies, the absorption (unoriented single crystals, KBr pellets) and luminescence (oriented single crystals, KBr pellets) of compounds **1** and **2** were recorded.

In Fig. 8, the absorption spectrum (room temperature) of an unoriented single crystal of **1** is compared with the 77 K absorption spectrum of a KBr pellet of **2** (at ambient temperature the signals of the latter compound are too weak). In the range 15 000–17 000 cm^{-1}, compound **1** exhibits two strong distinct peaks at ca. 15 360 and 16 590 cm^{-1} which are missing in the case of **2**. For this reason, they correspond to excitations of an f electron to energetically higher d or ligand orbitals.

In order to elucidate the experimental zero phonon energy of the transition initiating at $^2F_{5/2}$ and terminating at the lowest d level, we make use of the following definitions: the difference of energies of the fast absorption transition initiating at $^2F_{5/2}$ and thus terminating at vibronic levels of the lowest d level and (after some radiationless decays) the inverse luminescence transition is defined as Stokes shift of Ce^{III} compounds [9,37,38], and the mean value of both transitions indicates roughly the zero phonon transition [37]. This means that the energy of the (vibronic) $^2F_{5/2} \rightarrow 5d$ transition can be roughly estimated by adding the Stokes shift to the observed energy of the corresponding $5d \rightarrow {}^2F_{5/2}$ luminescence transition. For purposes of comparison with the predictions of the relativistic DV-Xα calculation the experimental zero phonon energy is estimated as the mean value of the energies of the absorption and the luminescence transition.

Applying the laser lines at 785, 632.8 and 532 nm of the Senterra Raman instrument to oriented single crystals of **1**, three strong at broad luminescence bands with maxima at ca. 11 800, 13 700 and 18 300 cm^{-1} appear, which show nearly negligible polarization effects. 5d → 4f luminescence transitions (initiating and the lowest d level) move between ca. 32 790 and 11 920 cm^{-1} [9, Table SI-3]. This did not allow spontaneously selection of the desired $5d \rightarrow {}^2F_{5/2}$ transition out of the above-mentioned luminescence energies. However, in a number of cases these d → f

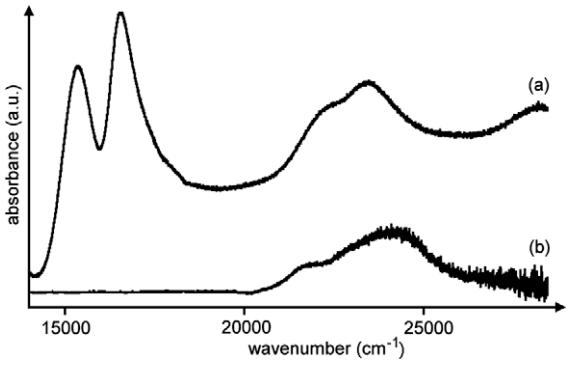

Fig. 8. Absorption spectra of $LnCp^*_3$ in the range 14 000–28 500 cm^{-1}: (a) Ln = Ce, unoriented single crystal, room temperature; (b) Ln = La, KBr pellet, ca. 77 K.

transitions are split into two components with the terminal multiplets $^2F_{5/2}$ and $^2F_{7/2}$, respectively, which are separated in the case of Ce^{III} organometallics between 1390 cm^{-1} ($[Li(THF)_4][Ce(\eta^8\text{-}C_8H_8)_2$ [39]) and 2330 cm^{-1} ($LiCp^*_2CeCl_2$ [40]) with 1900–1950 cm^{-1} being the most common values (see Ref. [9, Table SI-3]). Hence, the bands at 13 700 and 11 800 cm^{-1} (with ΔE = 1900 cm^{-1}) correspond most probably to the transitions initiating on the lowest d level $12e_{1/2}$ and terminating on $^2F_{5/2}$ and $^2F_{7/2}$, respectively. This pair of values is comparable with that of $[Li(THF)_4][Ce(\eta^8\text{-}C_8H_8)_2]$ (13 310/11 920 cm^{-1} [39]), the Ce^{III} compound with the strongest redshift of 5d → 4f transitions found to date [9, Table SI-3].

The only Stokes shift known for a Ce^{III} compound with organic ligands is that of $[(\eta^8 - C_8H_8)Ce(Tp^{Me_2})(THF)]$ with 1200 cm^{-1} [9]. Adopting tentatively this value for **1** and adding 1200 to 13 700 cm^{-1} one ends up with ca. 14 900 cm^{-1}. Hence, the absorption band with an energy of ca. 15 360 cm^{-1} and not that at ca. 16 590 cm^{-1} corresponds most probably to the searched for vibronic $^2F_{5/2}$ → 5d transition with the lowest energy. Combining this value with the energy of the vibronic luminescence transition 5d → $^2F_{5/2}$ (13 700 cm^{-1}), one arrives at a zero phonon value of ca. 14 530 cm^{-1}, which is approximately 2000 cm^{-1} lower than the predicted value (16 542 cm^{-1}) [17].

The adjacent band in the absorption spectrum with an energy of 16 590 cm^{-1}, which is due to an excitation of an f electron (vide supra), has no counterpart of a predicted transition in the relativistic DV-Xα calculation.

In the range 20 000–25 000 cm^{-1}, compounds **1** and **2** show comparable absorbance curves, namely a shoulder on the low energetic side of a broad band at ca. 22 620/23 485 and 22 000/24 300 cm^{-1}, respectively (both are missing in the case of $NaCp^*$), thus indicating that these signals are not caused by the excitation of an f electron. Possibly, the transition $(\eta\text{-}C_5H_5)\pi_2$ → $^2F_{5/2}$, which was predicted at 26 554 cm^{-1} by the relativistic DV-Xα calculation [17], is the reason for at least one of these signals. The difference between experiment and prediction may be explained by the expected red shift of this signal upon substitution of the $(\eta^5\text{-}C_5H_5)^-$ rings [17].

At ca. 27 000 cm^{-1}, the onset of a broad band with the maximum at ca. 28 200 cm^{-1} is visible in the case of **1**. Complex **2**, however, in this range shows a poor signal-to-noise ratio, which prevents the reliable detection of the corresponding signal. If it is indeed missing, the band at ca. 28 200 cm^{-1} in the absorption spectrum of **1** has to be correlated with the predicted $^2F_{5/2}$ → $(\eta^5\text{-}C_5H_5)\pi_3$ charge transfer transition at 27 660 cm^{-1} [17]. The small difference between experiment and theory may be explained by a blue shift upon functionalization of the ring [17].

The absorption spectrum of $Ce(C_5Me_4H)_3$ (KBr pellet) closely resembles that of **1** [12, Fig. 6]. However, that of similarly ψ trigonal planar $Ce\{\eta^5\text{-}C_5H_3(SiMe_3)_2)\}_3$ exhibits, instead of the two distinct peaks at 15 360 and 16 590 cm^{-1} and the diffuse ones at 22 620 and 23 485 cm^{-1} found for **1**, only two broad bands centred at 17 650 and 22 125 cm^{-1}, which were correlated with the transitions 4f → 5dσ and 4f → 5dπ, respectively [41]. In Ref. [17], that latter band was alternatively assigned to the above-mentioned transition $(\eta\text{-}C_5H_5)\pi_2$ → $^2F_{5/2}$, with a predicted energy of 26 554 cm^{-1}.

In case of YAG:Ce^{3+}, the $^2F_{5/2}$ → 5d absorption transitions in the UV–Vis range have energies of ca. 22 000, 30 000, 37 000 and 44 000 cm^{-1} [42]. The two lowest transitions have considerably higher energies than those of complex **1**, thus indicating that the ligand field splitting of d orbitals of this complex is lower than that of **1**.

5. Conclusions

In contrast to a number of other Ce^{III} compounds, the observation of bands of f → f transitions of complex **1** are not hampered by vibrational signals in the MIR spectrum. For this reason, the underlying CF splitting pattern could be derived by comparing the low temperature MIR spectra of **1** and **2**. The difference of the experimental energies of the barycenters of CF levels of the multiplets $^2F_{7/2}$ and $^2F_{5/2}$ is larger than in the gaseous Ce^{3+} free ion (experimental "anti"-relativistic nephelauxetic effect). However, fitting the free parameters of a phenomenological Hamiltonian for the complete f^1 configuration results in a ζ_{4f} value lower than that of Ce^{3+}, which corresponds to the expected relativistic nephelauxetic effect of a more covalent Ce^{III} compound.

The experimental CF splitting pattern of **1** is compared to the results of a relativistic DV-Xα calculation on the ψ trigonal planar model compound $Ce(\eta^5\text{-}C_5H_5)_3$. Although it is not expected that the substitution of the H atoms of the $\eta^5\text{-}C_5H_5$ rings with other groups should have a pronounced effect upon the essentially metal-localized electronic promotions [17], the calculated CF splitting pattern is by a factor of two larger than the experimental one. Besides, the calculation produces an incorrect CF ground state and an incorrect sequence of the CF levels of the excited multiplet $^2F_{7/2}$.

Likewise, the predicted transition initiating at $^2F_{5/2}$ and terminating at the lowest 5d level is off by ca. 2000 cm^{-1} and an additional sharp band which is due to the excitation of an f electron was not predicted. However, the agreement of experimental and calculated energies of two charge transfer bands is not too bad.

In order to identify experimentally detected f → f transitions of Ce^{III} compounds, it seems to be more appropriate to rely on experimental methods like polarized low temperature IR and electronic Raman spectroscopy of oriented single crystals than on relativistic model calculations. However, if these advanced methods are not available, identification calculations have to be performed which use the known CF parameters of the corresponding Pr^{III} or Nd^{III} compounds together with an adequate ζ_{4f} value.

Acknowledgements

The financial support of the "Deutsche Forschungsgemeinschaft" and the "US National Science Foundation" is gratefully acknowledged. We would like to thank the technicians U. Gralla, C. Bretzke and J. Walter for spectroscopic and Dr. Cigdem Capan and Professor Zachary Fisk for assistance with the SQUID measurements.

References

[1] H.-D. Amberger, H. Reddmann, T.J. Mueller, W.J. Evans, Organometallics, in press. doi:10.1021/om901007f.
[2] G.H. Dieke, Spectra and Energy Levels of Rare Earth Ions in Crystals, Interscience Publishers, New York, 1968. and references therein.
[3] C.A. Morrison, R.P. Leavitt, Spectroscopic properties of triply ionized lanthanides in transparent host materials, in: K.A. Gschneidner Jr., L. Eyring (Eds.), Handbook on the Physics and Chemistry of Rare Earths, vol. 5, North Holland Publishers, New York, 1982, pp. 461–692. and references therein (Chapter 46).
[4] C. Görller-Walrand, K. Binnemans, Rationalization of crystal field parameterization, in: K.A. Gschneidner Jr., L. Eyring (Eds.), Handbook on the Physics and Chemistry of Rare Earths, vol. 23, Elsevier, Amsterdam, 1996. and references therein (Chapter 155).
[5] G. Liu, B. Jacquier, Spectroscopic Properties of Rare Earths in Optical Materials, Springer-Verlag, Berlin, 2005. and references therein.
[6] J.A. Koningstein, O.S. Mortensen, Electronic Raman transitions, in: A. Anderson (Ed.), The Raman Effect, vol. 2, Dekker, New York, 1973, p. 519. and references therein.
[7] G. Schaack, Raman scattering by crystal-field excitations, Top. Appl. Phys., in: M. Cardona, G. Güntherodt (Eds.), Light Scattering in Solids VII, vol. 75, Springer-Verlag, Berlin-Heidelberg, 2000, pp. 24–173. and references therein.
[8] H.-D. Amberger, G.G. Rosenbauer, R.D. Fischer, Mol. Phys. 32 (1976) 1291.
[9] H.-D. Amberger, F.T. Edelmann, J. Gottfriedsen, R. Herbst-Irmer, S. Jank, U. Kilimann, M. Noltemeyer, H. Reddmann, M. Schäfer, Inorg. Chem. 48 (2009) 760.
[10] H. Reddmann, H. Schultze, H.-D. Amberger, C. Apostolidis, B. Kanellakopulos, Spectrochim. Acta 46A (1990) 1223.

[11] H.-D. Amberger, H. Reddmann, H. Schultze, S. Jank, B. Kanellakopulos, C. Apostolidis, Spectrochim. Acta, Part A 59 (2003) 2527.
[12] H. Reddmann, H.-D. Amberger, Z. Anorg. Allg. Chem. 634 (2008) 173.
[13] H.-D. Amberger, H. Reddmann, W.J. Evans, Inorg. Chem. 48 (2009) 10811.
[14] C.K. Jørgensen, The Nephelauxetic Series, Prog. Inorg. Chem. 73 (1962) 4.
[15] S. Jank, H.-D. Amberger, Acta Phys. Pol. A 90 (1996) 21.
[16] R.J. Strittmatter, B.E. Bursten, J. Am. Chem. Soc. 113 (1991) 552.
[17] N. Kaltsoyannis, B.E. Bursten, J. Organomet. Chem. 528 (1997) 19.
[18] W.J. Evans, J.M. Perotti, S.A. Kozimor, T.M. Champagne, B.L. Davis, G.W. Nyce, C.H. Fujimoto, R.D. Clark, M.A. Johnston, J.W. Ziller, Organometallics 24 (2005) 3916. and references therein.
[19] W.J. Evans, B.L. Davis, J.W. Ziller, Inorg. Chem. 40 (2001) 6341.
[20] W.J. Evans, D.B. Rego, J.W. Ziller, Inorg. Chem. 45 (2006) 10790.
[21] B.F. Gächter, J. Mol. Spectrosc. 63 (1976) 1. and references therein.
[22] J.H. van Vleck, Electric and Magnetic Susceptibilities, University Press, Oxford, 1932.
[23] K.W.H. Stevens, Proc. R. Soc. (London) 219 (1954) 542.
[24] W.T. Carnall, H. Crosswhite, H.M. Crosswhite, Energy Level Structure and Transition Probabilities in the Spectra of the Trivalent Lanthanides in LaF_3, ANL Report, 1977, unpublished, Supplement 1, Table 1.
[25] F. Auzel, O.L. Malta, J. Phys. (Paris) 44 (1983) 201.
[26] W.J. Evans, S.L. Gonzales, J.W. Ziller, J. Am. Chem. Soc. 113 (1991) 7423.
[27] W.J. Evans, C.A. Seibel, J.W. Ziller, J. Am. Chem. Soc. 120 (1998) 6745.
[28] H. Schumann, M. Glanz, H. Hemling, J. Organomet. Chem. 445 (1993) C1.
[29] H. Schumann, M. Glanz, H. Hemling, F.E. Hahn, Z. Anorg. Allg. Chem. 621 (1995) 341.
[30] R.J. Lang, Can. J. Res. 14 (1936) 127.
[31] K.H. Hellwege, E. Ohrlich, G. Schaack, Phys. Kondens. Mater. 4 (1965) 196.
[32] C.K. Jayasankar, F.S. Richardson, M.F. Reid, J. Less Common Met. 148 (1989) 289.
[33] W.T. Carnall, G.L. Goodman, K. Rajnak, R.S. Rana, J. Chem. Phys. 90 (1989) 3443.
[34] F.S. Richardson, M.F. Reid, J.J. Dallara, R.D. Smith, J. Chem. Phys. 83 (1985) 3813.
[35] G.F. Herrmann, J.J. Pearson, K.A. Wickersheim, R.A. Buchanan, J. Appl. Phys. 37 (1966) 1312.
[36] N.C. Chang, J.B. Gruber, R.P. Leavitt, C.A. Morrison, J. Chem. Phys. 76 (1982) 3877.
[37] G. Blasse, A. Bril, J. Chem. Phys. 47 (1967) 5139.
[38] B.F. Aull, H.P. Jenssen, Phys. Rev. B 34 (1986) 6647.
[39] H.-D. Amberger, H. Reddmann, F.T. Edelmann, J. Organomet. Chem. 690 (2005) 2238.
[40] P.N. Hazin, J.W. Bruno, H.-G. Brittain, Organometallics 6 (1987) 913.
[41] W. K. Kot, Dissertation, Lawrence Berkeley Laboratory, University of California, 1991.
[42] W.J. Miniscalco, J.M. Pellegrino, W.M. Yen, J. Appl. Phys. 49 (1978) 6109.